# Polariton Superfluids Reveal Quantum Hydrodynamic Solitons

A. Amo,[1,2]* S. Pigeon,[3] D. Sanvitto,[4] V. G. Sala,[1] R. Hivet,[1] I. Carusotto,[5] F. Pisanello,[1,4,6] G. Leménager,[1] R. Houdré,[7] E Giacobino,[1] C. Ciuti,[3] A. Bramati[1]*

A quantum fluid passing an obstacle behaves differently from a classical one. When the flow is slow enough, the quantum gas enters a superfluid regime, and neither whirlpools nor waves form around the obstacle. For higher flow velocities, it has been predicted that the perturbation induced by the defect gives rise to the turbulent emission of quantized vortices and to the nucleation of solitons. Using an interacting Bose gas of exciton-polaritons in a semiconductor microcavity, we report the transition from superfluidity to the hydrodynamic formation of oblique dark solitons and vortex streets in the wake of a potential barrier. The direct observation of these topological excitations provides key information on the mechanisms of superflow and shows the potential of polariton condensates for quantum turbulence studies.

Superfluidity is the remarkable property of flow without friction (*1*). It is characterized by the absence of excitations when the fluid hits a localized static obstacle at flow speeds $v_{flow}$ below some critical velocity $v_c$. For small potential barriers, the critical velocity is given by the Landau criterion as the minimum of $\omega(k)/k$, with $\omega(k)$ being the dispersion of elementary excitations in the fluid. In the case of dilute Bose-Einstein condensates (BECs), $v_c$ corresponds to $c_s$, the speed of sound of the quantum gas. For supersonic flows ($v_{flow} > c_s$), small obstacles induce dissipation (drag) via the emission of sound waves (*2*, *3*).

When the barrier is big, larger than the fluid's healing length—the minimum distance induced by particle interactions for changes in the density of the condensate—the density modulations caused by the barrier can generate topological excitations, such as vortices and solitons. These quantum hydrodynamic effects have been predicted to reduce the critical velocity (*4*, *5*).

Despite the amount of theoretical work (*4*–*6*), few experimental studies have addressed hydrodynamic features in atomic condensates through the observation of the break-up of superfluidity at fluid velocities lower than the speed of sound (*7*, *8*). Solitons in a quasi–one-dimensional (1D) geometry (*9*) and the nucleation of vortex pairs in an oblate BEC have been reported (*10*, *11*). Far from the hydrodynamic regime, formation of vortices and solitons has been shown by engineering the density and phase profile of the atomic condensate (*12*, *13*), or by the collision of two condensates (*14*).

Polariton superfluids appear promising in view of quantitative studies of quantum hydrodynamics. Polaritons are 2D composite bosons arising from the strong coupling between quantum well excitons and photons confined in a monolithic semiconductor microcavity. They possess an extremely small mass $m_{pol}$ on the order of $10^{-8}$ that of hydrogen, which allows for their Bose-Einstein condensation at temperatures ranging from a few kelvins (*15*) up to room temperature (*16*). All parameters of the system, such as the flow velocity, density, and shape and strength of the potential barriers, can be finely tuned with the use of just one (*3*) or two (*17*) resonant lasers, and by sample (*18*) or light-induced engineering (*19*). A crucial advantage with respect to atomic condensates is the possibility of fully reconstructing both the density and the phase pattern of the polariton condensate from the properties of the emitted light (*20*). This has been exploited in the recent observations of macroscopic coherence and long-range order (*15*, *18*, *21*), quantized vortices (*20*), superfluid flow past an obstacle (*3*, *17*, *22*), and persistent superfluid currents (*23*).

Here we use a polariton condensate to reveal quantum hydrodynamic features, whereby dark solitons and vortices are generated in the wake of a potential barrier. Following a recent theoretical proposal (*24*), we investigate different regimes at different flow speeds and densities, ranging from superfluidity to the turbulent emission of trains of vortices, and the formation of pairs of oblique dark solitons of high stability. For spatially large enough barriers, soliton quadruplets are also observed.

Our experiments are performed in an InGaAs-GaAs-AlGaAs microcavity at 10 K (*25*). We excite the system with a continuous-wave (cw) single-mode laser quasi-resonant with the lower polariton branch at an angle of incidence θ, resulting in the injection of a polariton fluid with a well-defined in-plane wave vector (*3*) ($k = k_0 \sin\theta$, where $k_0$ is the wave vector of the excitation laser field) and velocity $v_{flow} = k\hbar/m_{pol}$. The speed of sound of the fluid $c_s$ is related to the polariton density $|\psi|^2$ via the relation (*22*) $c_s = \sqrt{\hbar g|\psi|^2/m_{pol}}$, where $g$ is the polariton-polariton interaction constant.

Figure 1A shows the image of a polariton fluid with $k = 0.73\ \mu m^{-1}$ and $v_{flow} = 1.7\ \mu m/ps$, created with a Gaussian excitation spot 30 μm in diameter. The resonant pump is centered slightly upstream from a photonic defect of 4.5 μm present in the microcavity, in order not to lock the phase of the flowing condensate past the defect. Two oblique dark solitons with a width of 3 to 5 μm (Fig. 1B) are spontaneously generated in the wake of the barrier created by the defect and propagate within the polariton fluid in a straight line.

An unambiguous characteristic of solitons in BECs is the phase jump across the soliton (*12*, *13*, *26*). To reveal the phase variations in the polariton quantum fluid, we make the emission from the condensate interfere with a reference beam of homogeneous phase, with a given angle between the two beams (*20*). The result (Fig. 1C) shows a phase jump of up to π (half an interference period) as a discontinuity in the interference maxima along the soliton.

The 1D soliton relationships obtained from the solution of the Gross-Pitaevskii equation (*13*, *26*) can be extended to two dimensions to relate the soliton velocity $v_s$ in the reference frame of the fluid, the phase jump δ, and depth $n_s$ with respect to the polariton density $n$ away from the soliton:

$$\cos\left(\frac{\delta}{2}\right) = \left(1 - \frac{n_s}{n}\right)^{1/2} = \frac{v_s}{c_s} \qquad (1)$$

In our geometry, a soliton standing in a straight line in the laboratory frame implies a constant $v_s = v_{flow}\sin\alpha$, where α is defined in Fig. 1A. As the soliton becomes darker ($n_s$ approaching $n$), the phase jump saturates at $\delta = \pi$. Indeed, the solitons remain quite deep up to the first 40 μm of trajectory (Fig. 1, B and D), with a corresponding phase jump close to, but smaller than, π. At longer distances, the depth decreases along with the phase jump. Open triangles in Fig. 1D show the ratio $n_s/n$ as obtained from the measured phase jump and Eq. 1. This confirms that the soliton relationships, which were derived for condensates without dissipation (*26*), are applicable locally to the case of polaritons under cw pumping, where the polariton density is stationary in time. The polariton density continuously decreases downstream from the barrier due to the finite polariton

[1]Laboratoire Kastler Brossel, Université Pierre et Marie Curie-Paris 6, École Normale Supérieure et CNRS, UPMC Case 74, 4 place Jussieu, 75005 Paris, France. [2]CNRS–Laboratoire de Photonique et Nanostructures, Route de Nozay, 91460 Marcoussis, France. [3]Laboratoire Matériaux et Phénomènes Quantiques, UMR 7162, Université Paris Diderot-Paris 7 et CNRS, 75013 Paris, France. [4]NNL, Istituto Nanoscienze–CNR, Via Arnesano, 73100 Lecce, Italy. [5]INO-CNR BEC Center and Dipartimento di Fisica, Università di Trento, via Sommarive 14, I-38123 Povo, Italy. [6]Scuola Superiore ISUFI, Università del Salento, Via Arnesano, 73100 Lecce, Italy. [7]Institut de Physique de la Matière Condensée, Faculté des Sciences de Base, bâtiment de Physique, Station 3, EPFL, CH-1015 Lausanne, Switzerland.

*To whom correspondence should be addressed. E-mail: alberto.amo@lpn.cnrs.fr (A.A.); bramati@spectro.jussieu.fr (A.B.)

lifetime. This results in a decrease in the speed of sound (from $c_s = 3.5 \pm 1$ μm/ps at $\Delta y = 14$ μm, to $c_s = 1.2 \pm 0.5$ μm/ps at $\Delta y = 50$ μm [see (*25*) for the estimation of $c_s$], which compensates the expected acceleration of the soliton when it becomes less deep (smaller $n_s/n$ in Eq. 1). Consequently, the solitons present an almost rectilinear shape.

Simulations based on the Gross-Pitaevskii equation, with pumping and decay (*25*) according to the model described in (*24*) for the experimental parameters of Fig. 1, show the nucleation of a pair of solitons (Fig. 2A) with its associated phase jump (Fig. 2B). The model confirms that dark solitons nucleate hydrodynamically due to the gradient of flow speeds occurring around the potential barrier, which result in density variations on the order of the healing length. Once the soliton is formed, the repulsive interparticle interactions stabilize its shape as it propagates (*6*, *27*–*29*). By contrast, no stable soliton was observed at low excitation density when polariton-polariton interactions are negligible (see fig. S3).

Other hydrodynamic regimes can be explored by varying the mean polariton density (i.e., the speed of sound) for a fixed flow speed (Fig. 3). Here, polaritons move slower than in Fig. 1 ($v_{flow} =$ 0.79 μm/ps, $k = 0.34$ μm$^{-1}$), and due to their limited lifetime, they cannot propagate far away from the excitation spot. Hence, we have designed an excitation spot with the shape of half a Gaussian, with an abrupt intensity cut-off (fig. S1). Below the red line in Fig. 3, A to C, only polaritons propagating away from the pumped area are present, and their phase is not imposed by the resonant pump beam.

Figure 3A shows the polariton flow at subsonic speeds ($v_{flow} = 0.25\bar{c}_s$, where the bar indicates the mean speed of sound), at high excitation density. The condensate is in the superfluid regime, as evidenced by the absence of density modulations in the fluid hitting the barrier and from the homogeneous phase (Fig. 3D), showing a high value of the zero time first-order coherence (*25*), $g^{(1)}$ (Fig. 3G). When the excitation density and, correspondingly, the sound speed is decreased to $v_{flow} = 0.4\bar{c}_s$ (Fig. 3B), the fluid enters into a regime of turbulence characterized by the appearance of two low-density channels in the wake created by the barrier, with extended phase dislocations (Fig. 3E). We interpret this regime as corresponding to the continuous emission of pairs of quantized vortices and antivortices moving through those channels (*4*–*6*, *24*). Although a direct observation of the phase singularity of the emitted vortices is not possible under time-integrated cw experiments, the effects of the vortex flow are clearly seen when looking at $g^{(1)}$. Figure 3H shows a trace of low degree of coherence along each channel, due to the continuous passage of individual vortices. Finally, if the density is further decreased, we observe the formation of oblique dark solitons (Fig. 3C; $v_{flow} = 0.6\bar{c}_s$), with the characteristic phase jump along their trajectory (Fig. 3F), and a constant value of $g^{(1)}$ close to 1 (Fig. 3I).

The three regimes depicted in Fig. 3 have been anticipated by the nonequilibrium Gross-Pitaevskii model (*24*). We report a break-up of the superfluid regime at $v_{flow} \sim 0.4\bar{c}_s$, a value consistent with predictions for the onset of drag in the presence of large circular barriers (*4*, *5*). Our

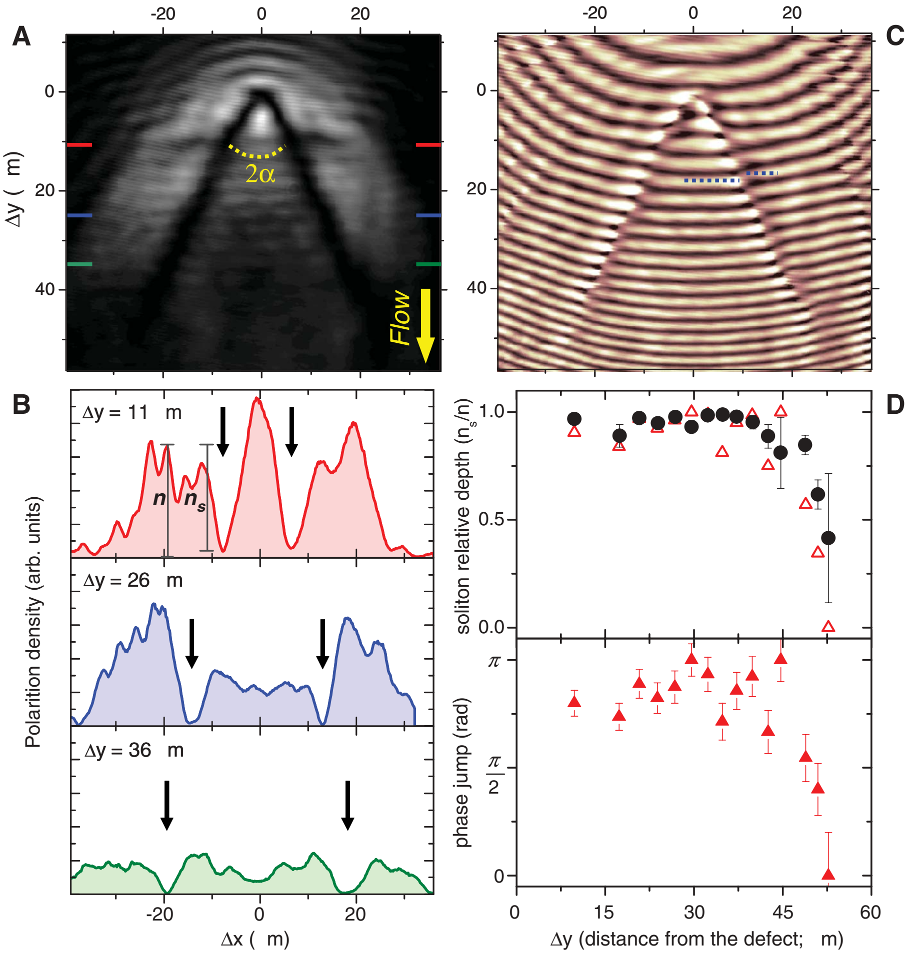


**Fig. 1.** (**A**) Real-space emission showing a soliton doublet nucleated in the wake of a photonic defect located at the origin. (**B**) Horizontal profiles at different downflow distances from the defect Δ*y*. Arrows indicate the soliton position. (**C**) Interference between the emitted intensity and a constant-phase reference beam, showing phase jumps along the solitons (dashed lines). The curved shaped of the fringes and the decreasing interfringe distance arise from the geometry of the reference beam. (**D**) Soliton depth (black circles) and phase jump obtained from (C) (filled triangles; see fig. S4), showing a strong correlation. Open triangles: soliton depth obtained from the measured phase jump and Eq. 1.

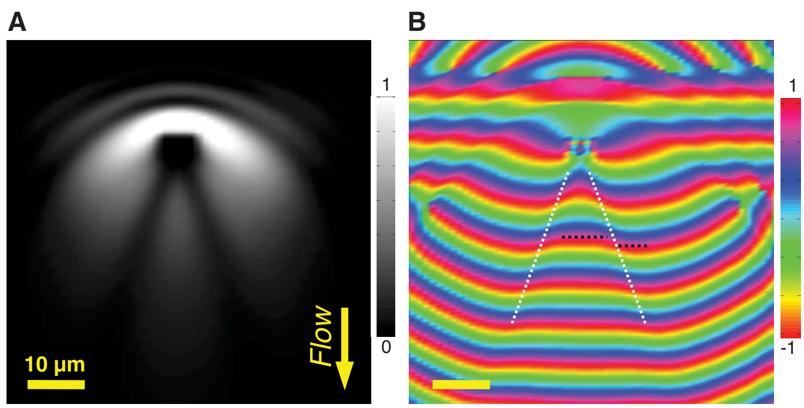


**Fig. 2.** (**A**) Real-space emission obtained from the solution of the nonequilibrium Gross-Pitaevskii equation for the parameters of the experiment depicted in Fig. 1. (**B**) Normalized real part of the polariton wave function, showing a phase jump (dark dashed lines) along the solitons (white dotted lines).

observations show that solitons in the polariton fluid can be stable down to subsonic speeds. This is in contrast to calculations for atomic condensates, in which oblique dark solitons are predicted to be stable only at supersonic speeds (*6*, *27*). Because our nonequilibrium simulations (Fig. 2) reproduce the observed nucleation at subsonic speeds, we infer that the additional damping in the polariton system arising from the finite lifetime is responsible for the stabilization of the soliton at subsonic speeds.

Finally, we have explored the possibility of going beyond the generation of soliton doublets by using a large circular potential barrier (*6*). Figure 4A shows a polariton flow at low momentum ($k = 0.2\ \mu\text{m}^{-1}$) injected in a Gaussian spot slightly above the obstacle, which nucleates a soliton doublet. If the momentum of the flow is increased above a certain value, the strong density mismatch before and after the defect can generate a soliton quadruplet (Fig. 4B, $k = 1.1\ \mu\text{m}^{-1}$). In principle, it should be possible to access even higher-order solitons by increasing both the obstacle size and the ratio $v_{\text{flow}}/c_s$.

Our results demonstrate the potential of polariton superfluids for experimental studies of quantum hydrodynamics. Both the velocity and the density of the quantum fluid can be finely controlled by optical means, and simultaneous access to the condensate density, phase, and coherence is available from the emitted light. These features have been essential in the reported observation of hydrodynamic generation of oblique solitons in the wake of potential barriers, and offer the opportunity to probe more complex phenomena like Andreev reflections (*30*), nucleation and trapping of vortex lattices (*24*), and quantum turbulence (*31*).

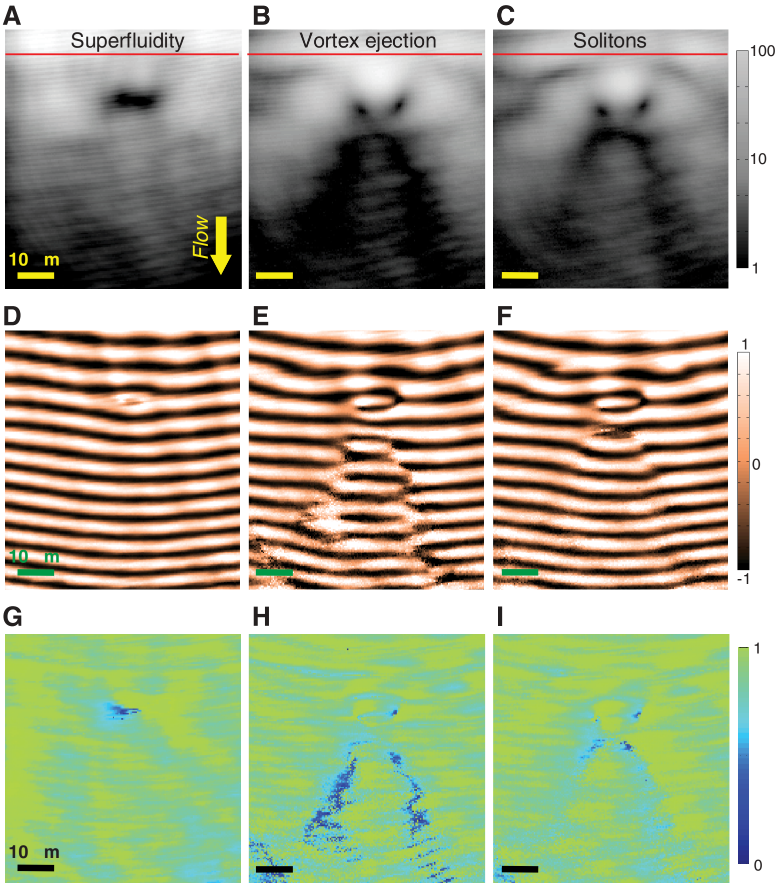


**Fig. 3.** (**A** to **C**) Real-space images of the polariton gas flowing downward at different excitation densities in the presence of a double defect (total width: 15 μm). The gas is injected above the red line (*25*). At high density (A) (117 mW), the fluid is subsonic ($v_{\text{flow}} = 0.25\bar{c}_s$) and flows in a superfluid fashion around the defect. At lower densities (B) (36 mW; $v_{\text{flow}} = 0.4\bar{c}_s$), a turbulent pattern appears in the wake of the defect, eventually giving rise to the formation of two oblique dark solitons (C) ($v_{\text{flow}} = 0.6\bar{c}_s$; 27 mW). (**D** to **F**) Interferograms corresponding to (A) to (C), respectively. (**G**) to (**I**) show the corresponding degree of first-order coherence [$g^{(1)}$, see (*25*)]. Saturated values of $g^{(1)}$ are due to the uncertainty in the measurements.

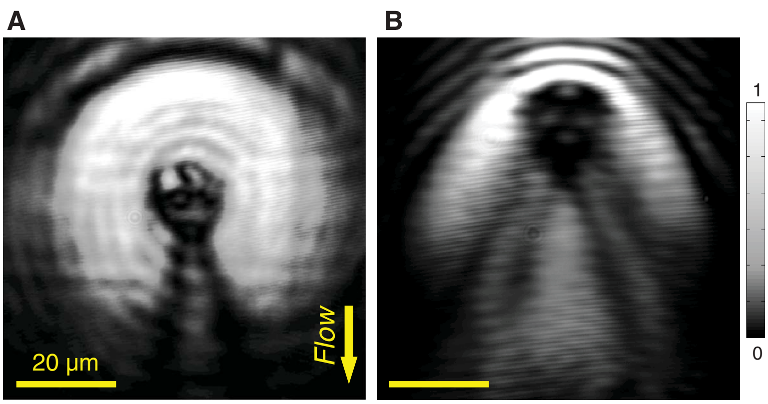


**Fig. 4.** Real-space images of the polariton flow around a large defect (17 μm in diameter) at low (**A**) ($k$ = 0.2 μm$^{-1}$) and high (**B**) ($k$ = 1.1 μm$^{-1}$) injected wave vectors showing, respectively, the formation of a soliton doublet and quadruplet.

### References and Notes


1. A. J. Leggett, *Rev. Mod. Phys.* **71**, S318 (1999).
2. I. Carusotto, S. X. Hu, L. A. Collins, A. Smerzi, *Phys. Rev. Lett.* **97**, 260403 (2006).
3. A. Amo *et al.*, *Nat. Phys.* **5**, 805 (2009).
4. T. Frisch, Y. Pomeau, S. Rica, *Phys. Rev. Lett.* **69**, 1644 (1992).
5. T. Winiecki, B. Jackson, J. F. McCann, C. S. Adams, *J. Phys. At. Mol. Opt. Phys.* **33**, 4069 (2000).
6. G. A. El, A. Gammal, A. M. Kamchatnov, *Phys. Rev. Lett.* **97**, 180405 (2006).
7. C. Raman *et al.*, *Phys. Rev. Lett.* **83**, 2502 (1999).
8. R. Onofrio *et al.*, *Phys. Rev. Lett.* **85**, 2228 (2000).
9. P. Engels, C. Atherton, *Phys. Rev. Lett.* **99**, 160405 (2007).
10. S. Inouye *et al.*, *Phys. Rev. Lett.* **87**, 080402 (2001).
11. T. W. Neely, E. C. Samson, A. S. Bradley, M. J. Davis, B. P. Anderson, *Phys. Rev. Lett.* **104**, 160401 (2010).
12. S. Burger, K. Bongs, S. Dettmer, W. Ertmer, K. Sengstock, *Phys. Rev. Lett.* **83**, 5198 (1999).
13. J. Denschlag *et al.*, *Science* **287**, 97 (2000).
14. J. J. Chang, P. Engels, M. A. Hoefer, *Phys. Rev. Lett.* **101**, 170404 (2008).
15. J. Kasprzak *et al.*, *Nature* **443**, 409 (2006).
16. S. Christopoulos *et al.*, *Phys. Rev. Lett.* **98**, 126405 (2007).
17. A. Amo *et al.*, *Nature* **457**, 291 (2009).
18. E. Wertz *et al.*, *Nat. Phys.* **6**, 860 (2010).
19. A. Amo *et al.*, *Phys. Rev. B* **82**, 081301 (2010).
20. K. G. Lagoudakis *et al.*, *Nat. Phys.* **4**, 706 (2008).
21. C. W. Lai *et al.*, *Nature* **450**, 529 (2007).
22. I. Carusotto, C. Ciuti, *Phys. Rev. Lett.* **93**, 166401 (2004).
23. D. Sanvitto *et al.*, *Nat. Phys.* **6**, 527 (2010).
24. S. Pigeon, I. Carusotto, C. Ciuti, *Phys. Rev. B* **83**, 144513 (2011).
25. Materials and methods are available on *Science* Online.
26. A. D. Jackson, G. M. Kavoulakis, C. J. Pethick, *Phys. Rev. A* **58**, 2417 (1998).
27. A. M. Kamchatnov, L. P. Pitaevskii, *Phys. Rev. Lett.* **100**, 160402 (2008).
28. A. V. Yulin, O. A. Egorov, F. Lederer, D. V. Skryabin, *Phys. Rev. A* **78**, 061801 (2008).

29. Y. Larionova, W. Stolz, C. O. Weiss, *Opt. Lett.* **33**, 321 (2008).
30. A. J. Daley, P. Zoller, B. Trauzettel, *Phys. Rev. Lett.* **100**, 110404 (2008).
31. N. G. Berloff, Turbulence in exciton-polariton condensates. Preprint available at http://arxiv.org/abs/1010.5225 (2010).

**Acknowledgments:** We thank S. Barbay, J. Bloch, R. Kuszelewicz, W. D. Phillips, L. P. Pitaevskii, and M. Wouters for useful discussions, and L. Martiradonna for the confocal masks. This work was supported by the IFRAF, CLERMONT4, and the Agence Nationale de la Recherche. A.B. and C.C. are members of the Institut Universitaire de France.

**Supporting Online Material**
www.sciencemag.org/cgi/content/full/332/6034/1167/DC1
Materials and Methods
Figs. S1 to S4

28 December 2010; accepted 11 April 2011
10.1126/science.1202307

# Observing the Average Trajectories of Single Photons in a Two-Slit Interferometer

**Sacha Kocsis,[1,2]* Boris Braverman,[1]* Sylvain Ravets,[3]* Martin J. Stevens,[4] Richard P. Mirin,[4] L. Krister Shalm,[1,5] Aephraim M. Steinberg[1]†**

A consequence of the quantum mechanical uncertainty principle is that one may not discuss the path or "trajectory" that a quantum particle takes, because any measurement of position irrevocably disturbs the momentum, and vice versa. Using weak measurements, however, it is possible to operationally define a set of trajectories for an ensemble of quantum particles. We sent single photons emitted by a quantum dot through a double-slit interferometer and reconstructed these trajectories by performing a weak measurement of the photon momentum, postselected according to the result of a strong measurement of photon position in a series of planes. The results provide an observationally grounded description of the propagation of subensembles of quantum particles in a two-slit interferometer.

In classical physics, the dynamics of a particle's evolution are governed by its position and velocity; to simultaneously know the particle's position and velocity is to know its past, present, and future. However, the Heisenberg uncertainty principle in quantum mechanics forbids simultaneous knowledge of the precise position and velocity of a particle. This makes it impossible to determine the trajectory of a single quantum particle in the same way as one would that of a classical particle: Any information gained about the quantum particle's position irrevocably alters its momentum (and vice versa) in a way that is fundamentally uncertain. One consequence is that in Young's double-slit experiment one cannot determine through which slit a particle passes (position) and still observe interference effects on a distant detection screen (equivalent to measuring the momentum). Particle-like trajectories and wavelike interference are "complementary" aspects of the behavior of a quantum system, and an experiment designed to observe one neces-

[1]Centre for Quantum Information and Quantum Control and Institute for Optical Sciences, Department of Physics, University of Toronto, 60 St. George Street, ON M5S 1A7, Canada. [2]Centre for Quantum Dynamics, Griffith University, Brisbane 4111, Australia. [3]Laboratoire Charles Fabry, Institut d'Optique, CNRS, Université Paris-Sud, Campus Polytechnique, 2 avenue Augustin Fresnel, RD 128, 91127 Palaiseau cedex, France. [4]National Institute of Standards and Technology, 325 Broadway, Boulder, CO 80305, USA. [5]Institute for Quantum Computing, University of Waterloo, 200 University Avenue West, Waterloo, ON N2L 3G1, Canada.

*These authors contributed equally to this work.
†To whom correspondence should be addressed. E-mail: steinberg@physics.utoronto.ca

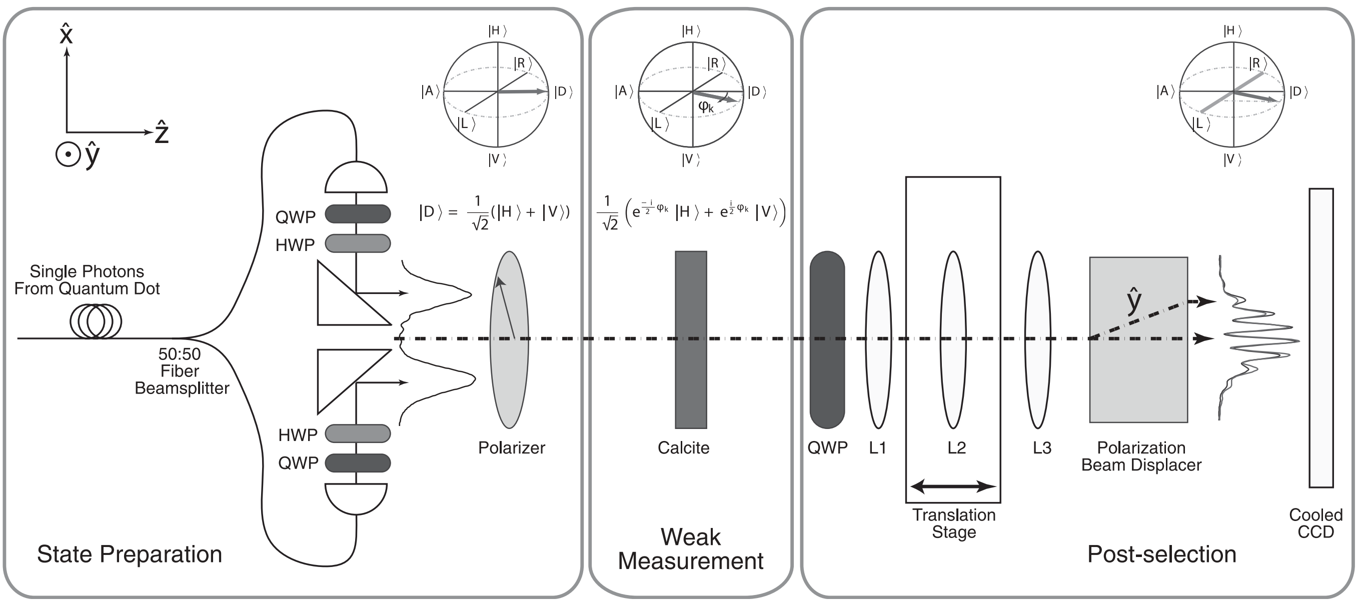


**Fig. 1.** Experimental setup for measuring the average photon trajectories. Single photons from an InGaAs quantum dot are split on a 50:50 beam splitter and then outcoupled from two collimated fiber couplers that act as double slits. A polarizer prepares the photons with a diagonal polarization $|D\rangle = \frac{1}{\sqrt{2}}(|H\rangle + |V\rangle)$. Quarter waveplates (QWP) and half waveplates (HWP) before the polarizer allow the number of photons passing through each slit to be varied. The weak measurement is performed by using a 0.7-mm-thick piece of calcite with its optic axis at 42° in the $x$-$z$ plane that rotates the polarization state to $\frac{1}{\sqrt{2}}(e^{-i\varphi_k/2}|H\rangle + e^{i\varphi_k/2}|V\rangle)$. A QWP and a beam displacer are used to measure the polarization of the photons in the circular basis, allowing the weak momentum value $k_x$ to be extracted. A cooled CCD measures the final $x$ position of the photons. Lenses L1, L2, and L3 allow different imaging planes to be measured. The polarization states of the photons are represented on the Poincaré sphere, where the six compass points correspond to the polarization states $|H\rangle, |V\rangle, |D\rangle, |A\rangle = \frac{1}{\sqrt{2}}(|H\rangle - |V\rangle), |L\rangle = \frac{1}{\sqrt{2}}(|H\rangle + i|V\rangle)$, and $|R\rangle = \frac{1}{\sqrt{2}}(|H\rangle - i|V\rangle)$.